ACS Photonics

Article

pubs.acs.org/journal/apchd5

Tetradymites as Natural Hyperbolic Materials for the Near-Infrared to Visible

Moritz Esslinger,*[,†,‡] Ralf Vogelgesang,*[,†,¶] Nahid Talebi,[†,§] Worawut Khunsin,[†,∥] Pascal Gehring,[†] Stefano de Zuani,[⊥] Bruno Gompf,[⊥] and Klaus Kern[†,#]

[†]Max-Planck-Institut für Festkörperforschung, 70569 Stuttgart, Germany

[‡]Fraunhofer-Institut für Angewandte Optik und Feinmechanik, Jena, Germany

[¶]Carl von Ossietzky Universität Oldenburg, 26129 Oldenburg, Germany

[§]Max-Planck-Institut für Intelligente Systeme, 70569 Stuttgart, Germany

[∥]The Blackett Laboratory, Department of Physics, Imperial College London, London SW7 2AZ, United Kingdom

[⊥]1. Physikalisches Institut, Universität Stuttgart, 70569 Stuttgart, Germany

[#]Institut de Physique de la Matière Condensée, École Polytechnique Fédérale de Lausanne, 1015 Lausanne, Switzerland

ABSTRACT: Hyperbolic media exhibit unparalleld properties, e.g, as light absorbers in photovoltaics and photonics, as superlenses in far-field imaging, as subwavelength light concentrators in nanolithography, or as novel materials in emission engineering. With the advent of optical metamaterials, deliberate design of material properties became possible. However, inadvertent variability in fabrication techniques and other factors limit performance characteristics of man-made hyperbolic materials. Here, we draw attention to a class of natural hyperbolic materials, the tetradymites. From generalized spectroscopic ellipsometry we extract the dielectric tensor components and find hyperbolic behavior in Bi_2Se_3 and Bi_2Te_3 in the near-infrared to visible spectrum. Previously, natural hyperbolic media were known only in the far-infrared spectral range. As possible applications of tetradymites we discuss superlenses for near-field microscopy and far-field isoindex filters. Solid solutions of tetradymites are likely tunable in operational wavelength from the infrared to the visible, complementing hyperbolic metamaterials.

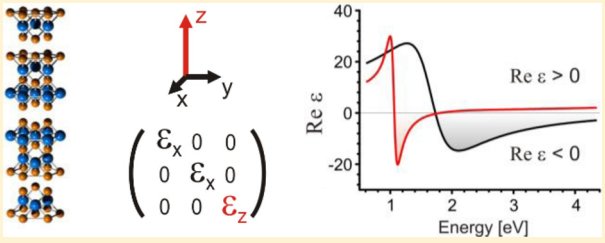

KEYWORDS: *hyperbolic materials, negative refraction, hyperresolved imaging, isoindex filters, thermophotovoltaics, near-field heat transfer*

The mineral tetradymite (Bi_2Te_2S) lends its name to a class of compounds with formula M_2X_3, where M = Bi, Sb and X = S, Se, Te. In particular, the topological insulator materials Bi_2Se_3 and Bi_2Te_3 have recently drawn considerable attention, thanks to their exceptional electronic surface states.[1] Common to all tetradymites is the layered structure made of atomic monolayer sequences $X_1-M-X_2-M-X_1$, which arrange themselves into hexagonal, quintuple layers. These, in turn, are stacked by weak van der Waals bonds to form flakes of bulk material, very similar to graphite being composed of graphene. Also single and few quintuple layer tetradymite structures are increasingly of interest.[2−5] The broader group of van der Waals materials and their combinatorial heterostructures have recently been highlighted for their potential to reveal many unusual properties and new phenomena.[6]

The layered nature of tetradymites gives rise to an exceedingly strong anisotropy in many material properties, including the electric permittivity. As we will show, due to their huge birefringence, materials from the tetradymite group belong to the rare class of natural, homogeneous *hyperbolic* materials. One notable other material is graphite at ultraviolet frequencies.[7−9] Strongly anisotropic polar phonon modes, e.g., in sapphire or calcite,[10−12] can also give rise to hyperbolic bands, particularly in the far-infrared. Tetradymites, however, suggest themselves for applications in the technologically relevant near-infrared to visible range. A comprehensive review of natural and man-made hyperbolic media has recently been published by Sun, Litchinitser, and Zhou.[13]

Conventionally, *elliptical* materials are used in applications of birefringent media such as spectral phase velocity and polarization management. Elliptical materials are characterized by all positive coefficients a in the dispersion relation $a_x k_x^2 + a_y k_y^2 + a_z k_z^2 = \omega^2/c^2$, which relates the wavevector $\vec{k}$ and angular frequency ω of plane waves in such media. Drastically different optical behavior is found in hyperbolic media, which have one (type I) or two (type II) negative coefficients.[14] On the basis of hyperbolic materials, a number of intriguing phenomena have been put forth recently, such as negative refraction and superfocusing,[7,15−18] hyperresolved imaging,[19−23] deep subwavelength lithography,[24−27] improved thermophotovoltaics

Received: August 11, 2014
Published: November 17, 2014

and super-Planckian near-field heat transfer,[28−33] control of single-quantum emitters,[34−37] novel types of bound surface and waveguide modes,[38,39] and optical forces.[40,41]

Artificial hyperbolic media may be fabricated as effective-medium- or meta-materials, e.g., by employing oriented nanowires, depositing alternating metallic/dielectric layers, or engineering quantum confinement in resonant semiconductor heterostructures.[15,16,18,21,36,42−47] This works particularly well for longer wavelengths, from the infrared even into the radio frequency range. At visible frequencies, however, besides issues with fabricating deeply subwavelength structures, strongly absorbing resonances often spoil useful hyperbolic properties. Here, we demonstrate that tetradymites indeed represent viable alternatives at these frequencies.

RESULTS AND DISCUSSION

Crystallographically, the tetradymites are characterized by a diagonal permittivity tensor with degenerate values in the *ab*-plane (*xy*) and a different one along the *c*-axis (*z*). Single crystals cleave with clean *ab*-facets, which provided easy access to the corresponding tensor components in extensive early spectroscopic reflectometry measurements.[48] The reported data for the permittivity component along the *c*-axis are less complete, though. To obtain a renewed, complete picture of the full permittivity tensor for the tetradymites Bi_2Se_3 and Bi_2Te_3, we perform generalized spectroscopic ellipsometry on single crystals in the energy range between 0.62 and 4.3 eV. The analysis of the recorded spectra displayed in Figure 1 shows that Bi_2Se_3 and Bi_2Te_3 are indeed strongly optically anisotropic.

In Bi_2Se_3 both independent permittivity components exhibit clearly separated absorption maxima at 1.05 for the *z*-component and 1.75 eV for the *xy*-component (see Figure 1b). These match very well with the energies of interband transitions at the Z- and F-point in the Brillouin zone, respectively.[1] Inspecting the Kramers−Kronig related real parts of the permittivity components (Figure 1d), we find that Bi_2Se_3 presents a rather extraordinary case of giant anisotropy. At energies between 1.05 and 1.75 eV, it exhibits negative real parts for the *z*-component of the permittivity tensor and positive *xy*-components. At 1.8 eV, this relation reverses, as the in-plane resonance becomes dominant. The real parts of the permittivity tensor components cross zero, and the tensor components exchange their respective roles. At higher energies, the in-plane *xy*-components are negative, while the out-of-plane *z*-component is positive. We note that the imaginary part of the *z*-component drops below 2.0 for energies above 1.55 eV.

As is evident from Figure 1c, Bi_2Te_3 also exhibits a strong anistropy in permittivity with distinct resonances in different directions. The resonances are at 0.9 eV for the out-of-plane and 1.2 eV for the degenerate in-plane components. Relative to Bi_2Se_3, both resonances occur at lower energies. As with Bi_2Se_3, there are energy intervals of hyperbolic anisotropy, where permittivity components in different directions have opposite sign. However, due to a weaker resonance in the *c*-direction, the out-of-plane permittivity real part below zero is less pronounced compared to Bi_2Se_3, as seen in Figure 1d,e.

In applications of uniaxial crystals like the tetradymites, there are two principal choices of surface orientation to consider: the *c*-axis may be perpendicular to the surface (*ab*-facets) or parallel to it (e.g., *ac*-facets). In either case, the dispersion for TM-polarized plane waves is given by

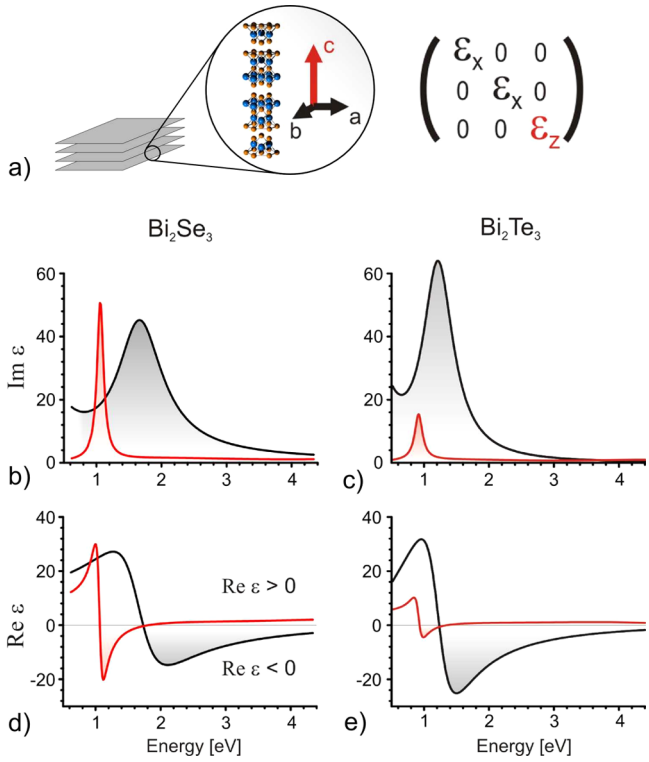

Figure 1. Crystal structure and permittivity tensor components of compounds from the tetradymite groups. (a) Quintuple atomic layers are stacked along the crystallographic *c*-axis by van der Waals forces. The zoom-in graphic shows the conventional hexagonal unit cell, which extends over three layers. The corresponding permittivity tensors are isotropic in the crystallographic *ab*-plane (indicated in black), but their perpendicular components (along the *c*-axis, indicated in red) are vastly different. (b ,c) Imaginary and (d, e) real parts of permittivity tensor components retrieved from generalized spectroscopic ellipsometry measurements of (b, d) Bi_2Se_3 and (c, e) Bi_2Te_3. The in-plane components are shown in black; the out-of-plane components in red.

$$\frac{k_{\parallel}^2}{\varepsilon_{\perp}} + \frac{k_{\perp}^2}{\varepsilon_{\parallel}} = k_0^2 \tag{1}$$

where $k_0 = \omega/c$ is the vacuum wavenumber and $k_{\parallel}$ and $k_{\perp}$ are respectively the wavevector components parallel and perpendicular to the surface. The parallel and perpendicular permittivity components are selected according to the material's tensor. On an *ac*-facet they are $(\epsilon_{\parallel},\epsilon_{\perp}) = (\epsilon_c,\epsilon_a)$, and we find type-II hyperbolic behavior in Bi_2Se_3 for energies above 2, as can be seen from the numerically evaluated dispersions presented in Figure 2a,b. In contrast, for the rotationally invariant *ab*-facets, the assignment $(\epsilon_{\parallel},\epsilon_{\perp}) = (\epsilon_a,\epsilon_c)$ implies type-I hyperbolic behavior in Bi_2Se_3 in the near-infrared range from 1.1 to 1.6 eV, as seen in Figure 2c,d.

Our findings suggest hyperresolved superlensing in the near-infrared to visible spectral regime as an intriguing possible application for hyperbolic tetradymites. Usually, type-I hyperbolic materials have lower reflection and perform better for high-resolution imaging than type II.[36] As this is also the easier facet to prepare, in the following we concentrate on superlensing slabs with *ab*-facets. We perform finite difference time domain (FDTD) simulations of a Bi_2Se_3 slab to test its imaging properties in a Rayleigh criterion configuration. As objects to be imaged two 20 nm wide slits in a gold film are

dx.doi.org/10.1021/ph500296e | ACS Photonics 2014, 1, 1285−1289

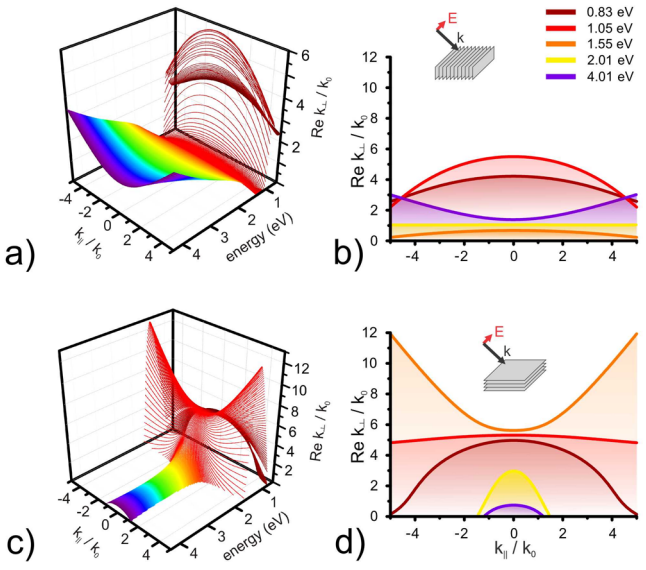

Figure 2. Plane wave dispersions in Bi_2Se_3 for TM-polarized light. In (a) and (b) the perpendicular direction is in the *ab*-plane; in (c) and (d) it is along the crystallographic *c*-axis. Panels (a) and (c) display a three-dimensional view of the dispersion relation eq 1; panels (b) and (d) present selected isoenergy cuts.

assumed, separated by a gap of 60 nm. They define the field at the input facet of an 80 nm thick Bi_2Se_3 slab. As seen in Figure 3, best performance is achieved at an energy of 1.06 eV (~1173 nm), i.e., in the anomalous response regime near the resonance in the *c*-direction. At 1.05 eV the imaginary part of ϵ_c is maximal, whereas its real part goes through zero. The transition

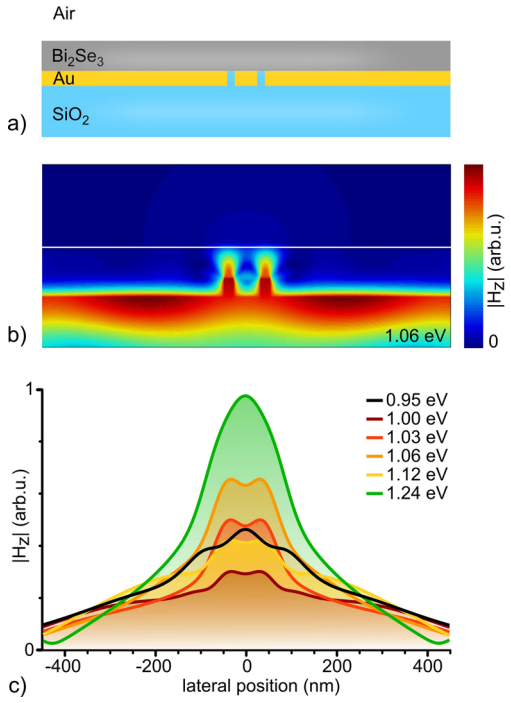

Figure 3. Imaging performance of a Bi_2Se_3 superlens slab. (a) A gold film with 20 slits, illuminated at normal incidence through the silicon dioxide substrate, is imaged by a 80 thick Bi_2Se_3 superlens toward the Bi_2Se_3–air interface. (b) $H_\perp$-field strength for excitation with $\lambda = 1.06$. The air–Bi_2Se_3 interface is indicated by a white line. (c) $H_\perp$ on the Bi_2Se_3–air interface for different excitation wavelengths.

from an elliptic to a hyperbolic dispersion occurs (see also Figure 2), which renders the dispersion curve flat (to third order) for $k_\parallel \approx 0$, and all spatial frequency components of the object field are transported in the normal direction with the same propagation wavenumber $k_\perp$. Hence the resulting image on the output facet exhibits two separated features of about ~50 nm in size, i.e., less than a twentieth of the excitation wavelength.

Another fascinating aspect of the strong anisotropy in tetradymites is the occurrence of pronounced isoindex points, i.e., energies for which (the real parts of) the refractive indices coincide accidentally for both dispersion branches. Only for excitation at exactly these isoindex energies do anisotropic materials appear isotropic. Plane waves in any direction are retarded with the same phase delay. However, for energies slightly off an isoindex point, the two differently polarized rays suffer very different phase delays, rapidly turning linear polarization into elliptical. Very narrow bandwidth filters ($\Delta\lambda < 0.1$) with a wide field-of-view (up to the full 2π sr) can be fabricated based on these drastic polarization rotation effects.[49,50] This kind of a spectrally narrow, omnidirectional filter is ideally suited for optical communication between moving objects, such as airplanes or submarines. Its performance depends critically on the slope $d(\Delta n)/d\lambda$ of the birefringent difference $\Delta n = n_1 - n_2$ of the indices of refraction at the isoindex wavelength λ_0. A useful figure of merit (FOM)[51] to compare isoindex points in different materials is

$$\mathrm{FOM} = \frac{1}{\lambda_0}\left|\frac{d(\Delta n)}{d\lambda}\right| \qquad (2)$$

As can be seen from Figure 1, Bi_2Te_3 has a single isoindex point at 1.24 eV, whereas in Bi_2Se_3 the ϵ_c resonance near 1.05 eV is strong enough to give rise to two additional isoindex points. The values listed in Table 1 indicate FOMs for tetradymites

Table 1. Figure of Merit for Frequency Filtering at the Isoindex Points ($n_1 = n_2$) of Bi_2Se_3 and Bi_2Te_3

material	energy (eV)	FOM (μm^{-2})
Bi_2Se_3	0.94	5.4
Bi_2Se_3	1.06	35
Bi_2Se_3	2.75	14
Bi_2Te_3	2.32	10
CdS[51]	2.36	2.3

that are even higher than that of CdS, one of the best materials available,[51] suggesting tetradymites as exquisite candidates for thinner or narrower wavelength filters.

CONCLUSION

In summary, our ellipsometry results show that tetradymites exhibit giant anisotropies in permittivity, which may be utilized in a variety of optical applications. The vastly different potential landscape electrons experience in the crystallographic *ab*-plane vs along the *c*-axis gives rise to energetically displaced interband transitions. These, in turn, lead to separate Lorentz-type resonances in different permittivity tensor components of sufficiently high quality factor that negative real parts are found over extended energy intervals. Chemically, this class of materials encompasses more than just the examples discussed in the present paper, and we expect similar properties to be found in many of them. A further advantage is their miscibility,

dx.doi.org/10.1021/ph500296e | ACS Photonics 2014, 1, 1285–1289

which should allow for tuning resonance energies and other properties relatively easily by deliberate growth of mixed crystals such as $Bi_2Se_{3-x}Te_x$.

We have discussed two possible applications of hyperbolic tetradymites. Hyperresolution imaging and lithography stand out as an immediate consequence of the drastic anisotropy. The enormous hyperbolic dispersions also suggest tetradymites as isoindex materials with superior figures of merit. These natural compounds and their mixed crystals may be a viable alternative to hyperbolic metamaterials and artificially fabricated metal/dielectric multilayers or multiple quantum-well structures. In contrast to laterally structured metamaterials, the dispersion of natural hyperbolic media extends much further in reciprocal space, due to their inherent atomic periodicity in real space. This results in increased densities of state, which may be exploited in near-field enhanced devices for heat management or photovoltaic effects. Finally, we note that tensorial hyperbolic/isotropic interfaces support bound surface modes that differ significantly from the surface plasmon polaritons found at scalar metal/dielectric interfaces,[52−54] which may provide new impetus for applications in the field of plasmonics.

METHODS

Ellipsometry. Optically, Bi_2Se_3 and Bi_2Te_3 were previously investigated by reflectometry methods,[48,55] accessing the degenerate permittivity components in the hexagonal planes, and infrared spectroscopic ellipsometry.[56] In this report, we optically characterize Bi_2Se_3 and Bi_2Te_3 single crystals grown by a vertical Bridgman method,[57] by ex-situ spectroscopic ellipsometry with a Woollam variable-angle spectroscopic ellipsometer (VASE). Measurements were performed at room temperature in the spectral range between 5000 and 35 000 cm^{-1} (0.62 to 4.3 eV) with a resolution of 100 cm^{-1} (12.4 meV), at angles of incidence from 55° to 75° in steps of 10°. Just before the measurement the samples were mechanically cleaved in order to avoid possible oxidation. The samples exhibit a sharp reflection spot, and in the ellipsometric analysis no hints for depolarization were found. Bi_2Se_3 and Bi_2Te_3 are uniaxial single crystals, characterized by an in-plane isotropy and an anisotropy along the z direction. To extract the dielectric functions from the measured ellipsometric angles, a single interface with no additional surface roughness or oxidation layer was used. The uniaxial model describing the in-plane permittivity consists of a Tauc−Lorentz oscillator with the energy gap at 0.29 eV, a Lorentz oscillator, and a Drude component. The general oscillator model describing the permittivity along the z direction is built by three Lorentz oscillators. Although ellipsometric measurements exhibit a limited sensitivity to out-of-plane anisotropies, measuring under various angles of incidence gives in the case of a single interface reliable results. The reflectivity, for example, calculated from the obtained dielectric functions is in very good agreement with previously published reflectivity data at normal incidence.[48]

Finite Difference Time Domain Method. For numerical simulations, we use our own finite difference time domain code with an analytical model for dispersion.[58] The anisotropy of the material is modeled by considering different permittivity values for lateral and vertical directions with our experimentally acquired permittivity data of Bi_2Se_3 (see Figure 1). The whole simulation domain is discretized by cubic Yee unit-cells of 5 nm size. For the outer boundaries, a higher order absorbing boundary condition is utilized.[59] It is noteworthy that this boundary condition is advantageous over the commonly used perfectly matched layers for large 3D simulations and allows the efficient use of the available memory for accurate numerical modeling of the main structure.

AUTHOR INFORMATION

Corresponding Authors

*E-mail: moritz.esslinger@uni-jena.de.
*E-mail: ralf.vogelgesang@uni-oldenburg.de.

Notes

The authors declare no competing financial interest.

REFERENCES

(1) Zhang, G.; Qin, H.; Teng, J.; Guo, J.; Guo, Q.; Dai, X.; Fang, Z.; Wu, K. Quintuplelayer epitaxy of thin lms of topological insulator Bi_2Se_3. *Appl. Phys. Lett.* **2009**, *95* (053114), 3.
(2) Zhang, H.; Liu, C.-X.; Qi, X.-L.; Dai, X.; Fang, Z.; Zhang, S.-C. Topological insulatorsin Bi_2Se_3, Bi_2Te_3 and Sb_2Te_3 with a single Dirac cone on the surface. *Nat. Phys.* **2009**, *5*, 438−442.
(3) Peng, H.; Lai, K.; Kong, D.; Meister, S.; Chen, Y.; Qi, X.-L.; Zhang, S.-C.; Shen, Z.-X.; Cui, Y. Aharonov-Bohm interference in topological insulator nanoribbons. *Nat. Mater.* **2010**, *9*, 225−229.
(4) Kong, D.; Dang, W.; Cha, J. J.; Li, H.; Meister, S.; Peng, H.; Liu, Z.; Cui, Y. Few-Layer nanoplates of Bi_2Se_3 and Bi_2Te_3 with highly tunable chemical potential. *Nano Lett.* **2010**, *10*, 2245−2250.
(5) Zhao, Y.; Chang, C.-Z.; Jiang, Y.; DaSilva, A.; Sun, Y.; Wang, H.; Xing, Y.; Wang, Y.; He, K.; Ma, X.; Xue, Q.-K.; Wang, J. Demonstration of surface transport in a hybrid Bi_2Se_3/Bi_2Te_3 heterostructure. *Sci. Rep.* **2013**, *3*, 3060.
(6) Geim, A. K.; Grigorieva, I. V. Van der Waals heterostructures. *Nature* **2013**, *499*, 419−425.
(7) Sun, J.; Zhou, J.; Li, B.; Kang, F. Indenite permittivity and negative refraction in natural material: graphite. *Appl. Phys. Lett.* **2011**, *98*, 101901.
(8) Marinopoulos, A. G.; Reining, L.; Olevano, V.; Rubio, A.; Pichler, T.; Liu, X.; Knupfer, M.; Fink, J. Anisotropy and interplane interactions in the dielectric response of graphite. *Phys. Rev. Lett.* **2002**, *89*, 076402.
(9) Warmbier, R.; Manyali, G. S.; Quandt, A. Surface plasmon polaritons in lossy uniaxial anisotropic materials. *Phys. Rev. B* **2012**, *85*, 085442.
(10) Thompson, D. W.; DeVries, M. J.; Tiwald, T. E.; Woollam, J. A. Determination of optical anisotropy in calcite from ultraviolet to midinfrared by generalized ellipsometry. *Thin Solid Films* **1998**, *313*, 341−346.
(11) Wang, R.; Sun, J.; Zhou, J. Indenite permittivity in uniaxial single crystal at infrared frequency. *Appl. Phys. Lett.* **2010**, *97*, 031912.
(12) Alekseyev, L. V.; Podolskiy, V. A.; Narimanov, E. E. Homogeneous hyperbolic systems for terahertz and far-infrared frequencies. *Adv. OptoElectron.* **2012**, 267564.
(13) Sun, J.; Litchinitser, N. M.; Zhou, J. Indefinite by nature: from ultraviolet to tera-hertz. *ACS Photonics* **2014**, *1*, 293−303.
(14) Drachev, V. P.; Podolskiy, V. A.; Kildishev, A. V. Hyperbolic metamaterials: new physics behind a classical problem. *Opt. Express* **2013**, *21*, 15048−15064.
(15) Hoffman, A. J.; Alekseyev, L.; Howard, S. S.; Franz, K. J.; Wasserman, D.; Podol-skiy, V. A.; Narimanov, E. E.; Sivco, D. L.; Gmachl, C. Negative refraction in semiconductor metamaterials. *Nat. Mater.* **2007**, *6*, 946−950.
(16) Yao, J.; Liu, Z.; Liu, Y.; Wang, Y.; Sun, C.; Bartal, G.; Stacy, A. M.; Zhang, X. Optical negative refraction in bulk metamaterials of nanowires. *Science* **2008**, *321*, 930−930.
(17) Fang, A.; Koschny, T.; Soukoulis, C. M. Optical anisotropic metamaterials: negative refraction and focusing. *Phys. Rev. B* **2009**, *79*, 245127.
(18) Naik, G. V.; Liu, J.; Kildishev, A. V.; Shalaev, V. M.; Boltasseva, A. Demonstration of Al:ZnO as a plasmonic component for near-

infrared metamaterials. *Proc. Natl. Acad. Sci. U.S.A.* **2012**, *109*, 8834−8838.
(19) Ramakrishna, S. A.; Pendry, J. B.; Wiltshire, M. C. K.; Stewart, W. J. Imaging the nearfield. *J. Mod. Opt.* **2003**, *50*, 1419−1430.
(20) Salandrino, A.; Engheta, N. Far-field subdiraction optical microscopy using metamaterial crystals: theory and simulations. *Phys. Rev. B* **2006**, *74*, 075103.
(21) Jacob, Z.; Alekseyev, L. V.; Narimanov, E. Optical hyperlens: far-field imaging beyond the diraction limit. *Opt. Express* **2006**, *14*, 8247−8256.
(22) Liu, Z.; Lee, H.; Xiong, Y.; Sun, C.; Zhang, X. Far-field optical hyperlens magnifying sub-diffraction-limited objects. *Science* **2007**, *315*, 1686−1686.
(23) Smolyaninov, I. I.; Hung, Y.-J.; Davis, C. C. Magnifying superlens in the visible frequency range. *Science* **2007**, *315*, 1699−1701.
(24) Xiong, Y.; Liu, Z.; Zhang, X. Projecting deep-subwavelength patterns from diffraction-limited masks using metal-dielectric multilayers. *Appl. Phys. Lett.* **2008**, *93*, 111116.
(25) Verslegers, L.; Catrysse, P. B.; Yu, Z.; Fan, S. Deep-subwavelength focusing and steering of light in an aperiodic metallic waveguide array. *Phys. Rev. Lett.* **2009**, *103*, 033902.
(26) Ma, C.; Liu, Z. A super resolution metalens with phase compensation mechanism. *Appl. Phys. Lett.* **2010**, *96*, 183103.
(27) Ishii, S.; Kildishev, A. V.; Narimanov, E.; Shalaev, V. M.; Drachev, V. P. Subwavelength interference pattern from volume plasmon polaritons in a hyperbolic medium. *Laser Photonics Rev.* **2013**, *7*, 265−271.
(28) Nefedov, I. S.; Simovski, C. R. Giant radiation heat transfer through micron gaps. *Phys. Rev. B* **2011**, *84*, 195459.
(29) Biehs, S. A.; Tschikin, M.; Ben-Abdallah, P. Hyperbolic metamaterials as an analog of a blackbody in the near field. *Phys. Rev. Lett.* **2012**, *109*, 104301.
(30) Guo, Y.; Cortes, C. L.; Molesky, S.; Jacob, Z. Broadband super-Planckian thermal emission from hyperbolic metamaterials. *Appl. Phys. Lett.* **2012**, *101*, 131106.
(31) Nefedov, I. S.; Valagiannopoulos, C. A.; Hashemi, S. M.; Nefedov, E. I. Total absorption in asymmetric hyperbolic media. *Sci. Rep.* **2013**, *3*, 2662.
(32) Simovski, C.; Maslovski, S.; Nefedov, I.; Tretyakov, S. Optimization of radiative heat transfer in hyperbolic metamaterials for thermophotovoltaic applications. *Opt. Express* **2013**, *21*, 14988−15013.
(33) Biehs, S. A.; Tschikin, M.; Messina, R.; Ben-Abdallah, P. Super-Planckian near-field thermal emission with phonon-polaritonic hyperbolic metamaterials. *Appl. Phys. Lett.* **2013**, *102*, 131106.
(34) Wood, B.; Pendry, J. B.; Tsai, D. P. Directed subwavelength imaging using a layered metal-dielectric system. *Phys. Rev. B* **2006**, *74*, 115116.
(35) Poddubny, A. N.; Belov, P. A.; Kivshar, Y. S. Spontaneous radiation of a finite-size dipole emitter in hyperbolic media. *Phys. Rev. A* **2011**, *84*, 023807.
(36) Cortes, C. L.; Newman, W.; Molesky, S.; Jacob, Z. Quantum nanophotonics using hyperbolic metamaterials. *J. Opt.* **2012**, *14*, 063001.
(37) Sreekanth, K. V.; Biaglow, T.; Strangi, G. Directional spontaneous emission enhancement in hyperbolic metamaterials. *J. Appl. Phys.* **2013**, *114*, 134306.
(38) He, Y.; He, S.; Yang, X. Optical field enhancement in nanoscale slot waveguides of hyperbolic metamaterials. *Opt. Lett.* **2012**, *37*, 2907−2909.
(39) Hu, H.; Ji, D.; Zeng, X.; Liu, K.; Gan, Q. Rainbow trapping in hyperbolic metamaterial waveguide. *Sci. Rep.* **2013**, *3*, 1249.
(40) He, Y.; He, S.; Gao, J.; Yang, X. Giant transverse optical forces in nanoscale slot waveguides of hyperbolic metamaterials. *Opt. Express* **2012**, *20*, 22372−22382.
(41) Ginzburg, P.; Krasavin, A. V.; Poddubny, A. N.; Belov, P. A.; Kivshar, Y. S.; Zayats, A. V. Self-induced torque in hyperbolic metamaterials. *Phys. Rev. Lett.* **2013**, *111*, 036804.
(42) Pendry, J. B.; Martin-Moreno, L.; Garcia-Vidal, F. J. Mimicking surface plasmons with structured surfaces. *Science* **2004**, *305*, 847−848.
(43) Cai, W. S.; Genov, D. A.; Shalaev, V. M. Superlens based on metaldielectric composites. *Phys. Rev. B* **2005**, *72*, 193101.
(44) Maier, S. A.; Atwater, H. A. Plasmonics: localization and guiding of electromagnetic energy in metal/dielectric structures. *J. Appl. Phys.* **2005**, *98*, 011101.
(45) Elser, J.; Wangberg, R.; Podolskiy, V. A.; Narimanov, E. E. Nanowire metamaterials with extreme optical anisotropy. *Appl. Phys. Lett.* **2006**, *89*, 261102.
(46) Noginov, M. A.; Li, H.; Barnakov, Y. A.; Dryden, D.; Nataraj, G.; Zhu, G.; Bonner, C. E.; Mayy, M.; Jacob, Z.; Narimanov, E. E. Controlling spontaneous emission with metamaterials. *Opt. Lett.* **2010**, *35*, 1863−1865.
(47) Yang, K. Y.; Giannini, V.; Bak, A. O.; Amrania, H.; Maier, S. A.; Phillips, C. C. Subwavelength imaging with quantum metamaterials. *Phys. Rev. B* **2012**, *86*, 075309.
(48) Greenaway, D. L.; Harbeke, G. Band structure of bismuth telluride, bismuth selenide and their respective alloys. *J. Phys. Chem. Solids* **1965**, *26*, 1585−1604.
(49) Henry, C. H. Coupling of electromagnetic waves in CdS. *Phys. Rev.* **1966**, *143*, 627−633.
(50) Yeh, P. Zero crossing birefringent filters. *Opt. Commun.* **1980**, *35*, 15−19.
(51) Henderson, D. M. A figure of merit for iso-index filter materials. *IEEE J. Quantum Electron.* **1982**, *18*, 921−925.
(52) Lyubimov, V. N.; Sannikov, D. G. Surface electromagnetic waves in a uniaxial crystal. *Soviet Phys. - Solid State* **1972**, *14*, 575−579.
(53) Wallis, R. F.; Brion, J. J.; Burstein, E.; Hartstei, A. Theory of surface polaritons in anisotropic dielectric media with application to surface magnetoplasmons in semiconductors. *Phys. Rev. B* **1974**, *9*, 3424−3437.
(54) Liscidini, M.; Sipe, J. E. Quasiguided surface plasmon excitations in anisotropic materials. *Phys. Rev. B* **2010**, *81*, 115335.
(55) Kohler, H.; Becker, C. R. Optically Active Lattice Vibrations in Bi_2Se_3. *Phys. Status Solidi B* **1974**, *61*, 533−537.
(56) LaForge, A. D.; Frenzel, A.; Pursley, B. C.; Lin, T.; Liu, X.; Shi, J.; Basov, D. N. Optical characterization of Bi_2Se_3 in a magnetic field: infrared evidence for magnetoelectric coupling in a topological insulator material. *Phys. Rev. B* **2010**, *81*, 125120.
(57) Benia, H. M.; Lin, C.; Kern, K.; Ast, C. R. Reactive chemical doping of the Bi_2Se_3 topological insulator. *Phys. Rev. Lett.* **2011**, *107*, 177602.
(58) Etchegoin, P. G.; Le Ru, E. C.; Meyer, M. An analytic model for the optical properties of gold. *J. Chem. Phys.* **2006**, *125*, 164705.
(59) Tirkas, P. A.; Balanis, C. A.; Renaut, R. A. Higher order absorbing boundary conditions for the finite-difference time-domain method. *IEEE Trans. Antennas Propag.* **1992**, *40*, 1215−1222.